View metadata, citation and similar papers at core.ac.uk

brought to you by CORE

provided by Explore Bristol Research

Stern, Juli, V., Osinga, H. M., LeBeau, A., & Sherman, A. (2007). Resetting behavior in a model of bursting in secretory pituitary cells: Distinguishing plateaus from pseudo-plateaus.

Early version, also known as pre-print

Link to publication record in Explore Bristol Research

PDF-document

University of Bristol - Explore Bristol Research

General rights

This document is made available in accordance with publisher policies. Please cite only the published version using the reference above. Full terms of use are available:
http://www.bristol.ac.uk/pure/about/ebr-terms.html

To appear in Bulletin of Mathematical Biology

Resetting Behavior in a Model of Bursting in Secretory Pituitary Cells: Distinguishing Plateaus from Pseudo-Plateaus

Julie V. Stern[a,c], Hinke M. Osinga[b,c], Andrew LeBeau[a], Arthur Sherman[a]

[a] *Laboratory of Biological Modeling, National Institute of Diabetes and Digestive and Kidney Diseases, National Institutes of Health, Bethesda, MD, USA* [b] *Bristol Centre for Applied Nonlinear Mathematics, Department of Engineering Mathematics, University of Bristol, Bristol, UK*

[c] These two authors contributed equally.

Abstract We study a recently discovered class of models for plateau bursting, inspired by models for endocrine pituitary cells. In contrast to classical models for fold-homoclinic (square-wave) bursting, the spikes of the active phase are not supported by limit cycles of the frozen fast subsystem, but are transient oscillations generated by unstable limit cycles emanating from a subcritical Hopf bifurcation around a stable steady state. Experimental timecourses are suggestive of such fold-subHopf models because the spikes tend to be small and variable in amplitude; we call this *pseudo-plateau* bursting. We show here that distinct properties of the response to attempted resets from the silent phase to the active phase provide a clearer, qualitative criterion for choosing between the two classes of models. The fold-homoclinic class is characterized by induced active phases that increase towards the duration of the unperturbed active phase as resets are delivered later in the silent phase. For the fold-subHopf class of pseudo-plateau bursting, resetting is difficult and succeeds only in limited windows of the silent phase but, paradoxically, can dramatically exceed the native active phase duration.

Keywords Bursting · Calcium oscillations · Pituitary · Stable and unstable manifolds · Fast-slow systems

1 Introduction

Bursting is a ubiquitous phenomenon found in electrically excitable cells, consisting of a slow alternation between a depolarized spiking or active phase and a hyperpolarize low-voltage or silent phase. Slow is a relative term, meaning slow compared to the timescale of the spiking. From a physiological point of view, bursting appears, in general, to be a way for cells to construct slow oscillations out of fast oscillations. Burst periods range from less than a second in fast cortical neurons, for which bursting has been suggested to enhance the reliability of synaptic transmission (Lisman 1997), to tens of seconds or minutes in secretory cells, which modulate organismal homeostasis over the course of a day. The bursting patterns that cells exhibit are diverse both in appearance and in the ionic mechanisms that produce them, but considerable progress has been made in developing a general theory that ties them together (Rinzel 1987; Bertram et al 1995; Izhikevich 2000; Golubitsky et al 2001).

A pattern of particular interest is the "square-wave" burst, which was among the first to be understood because it looks like a relaxation oscillation but with spikes superimposed on the depolarized plateau. Indeed, by averaging the fast equations, one can derive an equivalent relaxation oscillator system that is a good approximation to the original bursting system (Bertram et al 1995). When the spikes are initiated by calcium currents, as is generally the case in endocrine cells, such plateaus enable the cell to generate maintained elevations of cytosolic Ca^{2+}, which are very effective at driving secretion. Two well-studied examples of non-endocrine square wave bursting are the pacemaker neurons of the pre-Bötzinger complex, whose bursts of Na^{+} spikes underlie the respiratory rhythm (Butera et al 1999) and the chick spinal cord (Tabak et al 2000).

Here we introduce a generic model for bursting in pituitary secretory cells, adapted from a previous model for the pituitary corticotroph (LeBeau et al 1998). The model exhibits what we call pseudo-plateau bursting, because the plateau is not necessarily attracting throughout the active phase. A typical experimental recording from a pituitary somatotroph, which secretes growth hormone, is shown in Fig. 1. Note the short period (< 5 s), the small amplitude of the spikes on the plateaus and the sawtooth shape of the cytosolic Ca^{2+} timecourse, which strongly suggests that the rise in $[Ca^{2+}]_i$ is the agent that terminates each active phase.

Similar patterns have been observed in other pituitary cells, such as lactotrophs (Stojilkovic et al 2005, Fig. 4), which secrete prolactin, and corticotrophs (Kuryshev et al 1996, Fig. 3), which secrete adrenocorticotrophic hormone. Another pituitary cell, the gonadotroph, which secretes luteinizing hormone and follicle stimulating hormone, does not show spontaneous bursting, but simulations suggest that it could if it were augmented with a large-conductance (BK) Ca^{2+}- and voltage-activated K^{+} channel (van Goor et al 2001).

Another much studied example is the pancreatic β-cell, which secretes insulin. It shows a similar pattern to its pituitary cousins when recorded in isolation and has a short period (Kinard et al 1999, Fig. 3). In the more physiological situation, in which β-cells are situated in the electrically coupled islets of Langerhans, the bursts have periods of tens of seconds to minutes and taller spikes (Kinard et al 1999, Fig. 1).

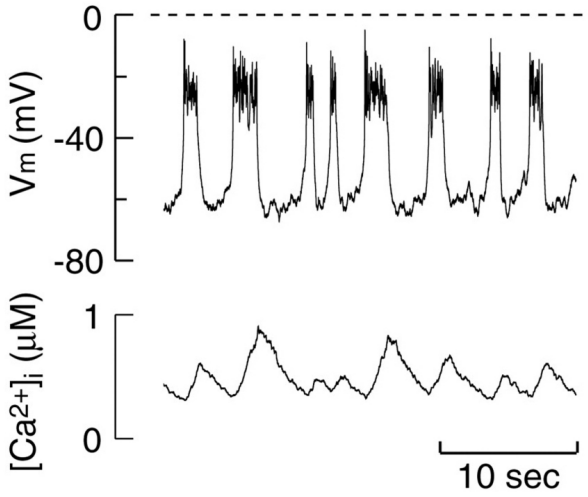

Fig. 1 A representative recording of membrane potential (upper) and cytosolic Ca^{2+} (lower) from a rat pituitary somatotroph using the perforated patch-clamp recording configuration in the current-clamp mode. (Reprinted with permission from Fig. 1, van Goor et al, J. Neurosci., 21(16):5902-5915. Copyright 2001 by the Society for Neuroscience.)

The β-cell was the first square-wave burster to be modeled (Chay and Keizer 1983), and a simulation of a version of that model (Sherman et al 1988) is shown in Fig. 2(a). We will refer to this model as "Chay-Keizer," although it differs in a number of details from the original, because it shares the key feature that the sole slow negative feedback variable is cytosolic Ca^{2+} acting on a Ca^{2+}-activated K^+ (K(Ca)) channel.

Alongside the Chay-Keizer simulation is one done with the pituitary model in Fig. 2(b). Both models produce square-wave bursts driven by Ca^{2+} acting on K(Ca) channels and have similar ion channels for spiking. The pituitary model output resembles the somatotroph data in Fig. 1 somewhat better than that of Chay-Keizer in that the spikes on the plateau are smaller, but the differences are not clear cut enough to be decisive. Experience has also shown that the appearance of the time course can be deceptive (Bertram et al 1995). The more critical difference between the two models, which can be taken as representative of two classes of models, is in the bifurcation diagrams of the respective fast subsystems, as described below.

In this study we show that even if the data are not precise enough to choose between the two classes of models quantitatively, they can be distinguished qualitatively by their resetting properties, that is, by the ability of brief perturbations to switch the system from the active to the silent phase and *vice versa*. The Chay-Keizer model resets in essentially the same manner as a relaxation oscillator, but the pituitary model turns out to be rather different. Thus, resetting offers an experimentally feasible way to distinguish which is the appropriate class of model to use for pituitary cells and other cells that show similar voltage patterns.

This paper is organized as follows. In the next section we present the system equations for the pituitary model and describe the techniques used for the analysis; complete details and values of the parameters are given in the Appendix. Section 3 gives detailed results of the behavior of the pituitary model. We first contrast the possibilities for upward resetting of the Chay-Keizer and the pituitary models in Section 3.1, which is determined by the bifurcation structure of the respective fast subsystems. We then continue with a detailed discussion of the effects of upward resetting on the pituitary model both in the fast subsystem with *Ca* frozen (Section 3.2) and in the full system with dynamic *Ca* (Section 3.3). We end with an extensive discussion in Section 4, starting with a summary of the results in Section 4.1. Section 4.2 addresses the robustness of the results. We explain the consequences both from a theoretical and an experimental point of view in Sections 4.3 and 4.4, respectively.

2 Modeling and Methods

The model used here was developed by modifying a previously published model for the pituitary corticotroph (LeBeau et al 1998). Our aim is to explore the potentially rich dynamical behavior that pituitary cells can display. Therefore, we simplified the model and reduced the number of variables only to the extent that existing numerical tools are able to tackle the analysis. In this way, the complexity of the model still reflects the actual biological system. The model is described by four differential equations, one for membrane potential, two for channel gating using the Hodgkin-Huxley formalism, and one for calcium balance:

$$C_m \frac{dV}{dt} = -I_{\mathrm{CaL}}(V, m_{\mathrm{L}}) - I_{\mathrm{CaT}}(V) - I_{\mathrm{K}}(V, n) - I_{\mathrm{KCa}}(V, Ca) - I_{\mathrm{Leak}}(V) + I_{\mathrm{app}}, \quad (1)$$

$$\frac{dm_{\mathrm{L}}}{dt} = \frac{m_{\mathrm{L},\infty}(V) - m_{\mathrm{L}}}{\tau_{m,\mathrm{L}}(V)}, \quad (2)$$

$$\frac{dn}{dt} = \frac{n_\infty(V) - n}{\tau_n}, \quad (3)$$

$$\frac{dCa}{dt} = J_{\mathrm{exchange}} + f\beta(J_{\mathrm{influx}} - J_{\mathrm{efflux}}). \quad (4)$$

The details of parameters and auxiliary activation, inactivation, and time functions for channel gating are in the Appendix. Source files can be downloaded from `http://lbm.niddk.nih.gov/sherman`.

Dynamically, the equations partition into a fast subsystem, consisting of V, m_{L}, and n, that is responsible for the spikes on the plateau, and a slow subsystem, consisting of Ca, that drives the system between active and silent phases. In the fast system for fixed (frozen) Ca the active and silent phases are identified by (stable) steady states, which we call the high-voltage and low-voltage states, respectively. The identification of Ca as the slow negative feedback variable that drives the bursts is suggested by the sawtooth Ca waveform (Fig. 1). By itself this waveform is not decisive, as Ca could just be following V, instead of driving V. In the somatotroph,

however, there is direct evidence supporting this mechanism, because the Ca^{2+} chelator BAPTA suppresses the $[Ca^{2+}]_i$ rise and kills the bursts (van Goor et al 2001, Fig. 3).

For comparison with classical square-wave bursting models, we show some results with a simplified form of the Chay-Keizer model for pancreatic β-cells (Sherman et al 1988). Like the pituitary model, the Chay-Keizer model has a fast subsystem for the spiking dynamics, which are driven by voltage-dependent Ca^{2+} and K^+ currents, and a slow subsystem consisting of Ca, which provides negative feedback onto K(Ca) current to switch the spikes on and off. The models differ in parameter values and in some details. For example, the Chay-Keizer model has no T-type Ca^{2+} current, only the L-type current, and the version used here has only three variables because the gating variable m_L for that current is set to its steady-state value. However, the only differences that matter for our purposes are in the bifurcation structure of the fast subsystem; see Fig. 2(c and d).

We use several techniques to analyse the models. Resetting experiments are simulated by briefly turning on the applied current I_{app} in Eq. (1). These simulations are carried out by integrating the equations using Matlab (The MathWorks, Natick, MA) or XPP (Ermentrout 2002). The bifurcation diagrams of the fast subsystem are computed using AUTO (Doedel 1981). Finally, an important part of our analysis involves the computation of global invariant manifolds for fixed Ca-values in the fast subsystem. In the three-dimensional fast subsystem (1)–(3) the two-dimensional global stable manifolds of a saddle equilibrium or a saddle periodic orbit are of interest, because these may separate the basins of attraction of the low- and high-voltage steady states.

The computation of two-dimensional global manifolds is a serious challenge, especially for systems with multiple time scales, and appropriate computational techniques have only recently become available (Krauskopf et al 2005). Our analysis, therefore, also provides for the first time insight into higher-dimensional effects on the phase-resetting of excitable cells. We find that for the pituitary model the effects are only at a quantitative level and the qualitative structure remains intact. We computed the two-dimensional global manifolds with the specialized method GLOBALIZEBVP (England et al 2007; Krauskopf and Osinga 2003) that builds the surface up as a collection of geodesic level sets, that is, a collection of closed curves (topological circles) with the property that points on the same curve lie at the same geodesic distance from the equilibrium or periodic orbit. The geodesic distance is the arclength of the shortest path on the manifold that connects the two objects, which need not be a trajectory. Hence, GLOBALIZEBVP computes the manifold as a geometric object and ignores the dynamics on it. The key step in this method is the observation that points on a geodesic level set can be found as end points of orbit segments that are the solution of a two-point boundary value problem. These two-point boundary value problems are solved by continuation using the collocation routines in AUTO, which makes the method particularly suitable for systems with multiple time scales. We refer to England et al (2007) for more details. Visualization of the manifolds was done in GEOMVIEW (Phillips et al 1993).

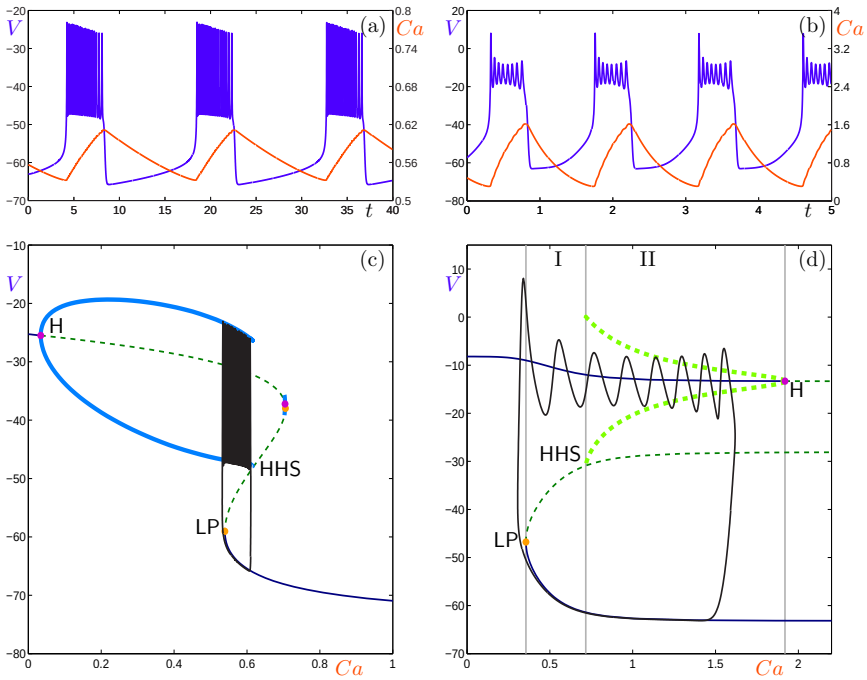

Fig. 2 The bursting profile for the Chay-Keizer model (left column) compared with that for the pituitary model (right column). Panels (a) and (b) show V (*purple*, left axis) and Ca (*orange*, right axis) versus t. Panels (c) and (d) show these orbits in the (Ca,V)-plane overlaid on the bifurcation diagrams of the corresponding fast subsystems.

3 Results

The results of our numerical analysis are presented in the following sections. We first discuss the bifurcation diagrams of the fast subsystem of the pituitary model and compare it with that of the Chay-Keizer model. We then focus on upward resetting in Sections 3.2 and 3.3. Section 3.2 concentrates on resetting in the frozen system, where Ca acts as a parameter. These results give qualitative information about the effects of resetting in the full dynamic case, which we discuss in Section 3.3.

3.1 Contrast of dynamical structure of Chay-Keizer and pituitary models

The bifurcation diagrams of the fast subsystems for the Chay-Keizer and pituitary models are compared in Fig. 2(c and d), respectively. In Chay-Keizer, bursting is due to the combination of slow negative feedback mediated by cytosolic Ca^{2+} with bistability between a low-voltage steady state and a high-voltage oscillatory state, the latter consisting of a one-parameter family of stable limit cycles. In the pituitary model, bursting is similarly dependent on slow negative feedback and hysteresis between the low- and high-voltage states, but the active-phase limit cycles are saddle periodic orbits. Thus, the spikes (or spikelets) are generated by transient oscillations

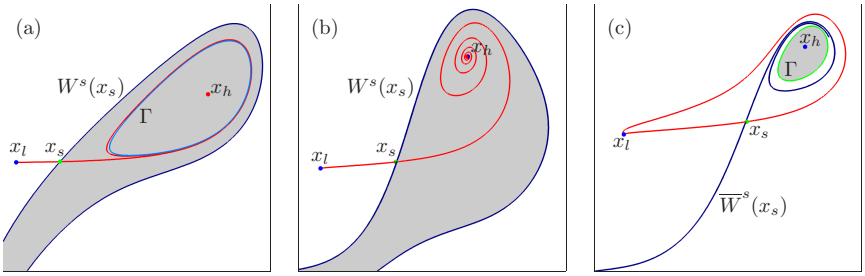

Fig. 3 Basins of attraction (shaded) of the depolarized state x_h in the fast subsystem. Panel (a) shows the Chay-Keizer model with $Ca = 0.55$. Panel (b) shows a projection of a similarly large basin for the pituitary model with $Ca = 0.55$ (region I in Fig. 2(d)), but the basin is dramatically smaller for the pituitary model at $Ca = 1.0$ (region II in Fig. 2(d)) shown in panel c. In each panel the horizontal axis is V and the vertical axis is n. The periodic orbit and the high-voltage, low-voltage and saddle steady states are labeled Γ, x_h, x_l, and x_s, respectively. Panel (a) shows the one-dimensional stable and unstable manifolds $W^s(x_s)$ and $W^u(x_s)$ of x_s, respectively, while panels (b) and (c) show projections of the one-dimensional unstable manifold $W^u(x_s)$ and a one-dimensional slice $\overline{W}^s(x_s)$ of the two-dimensional stable manifold of x_s.

around a stable high-voltage steady state. In order to obtain spikes in such a case, the slow variable (Ca) cannot be too slow; if Ca were very slow, the trajectory would compress onto the high-voltage steady-state branch, producing a flat plateau without spikes. This constraint does not generally apply to Chay-Keizer, where a slowing down of Ca just increases the number of spikes per burst, although there are marginal cases in which the speed of the slow variable matters.

In the terminology of Izhikevich (2000), Chay-Keizer is classified as a fold-homoclinic burster because the active phase begins at a fold (LP) and terminates at a homoclinic orbit of a saddle steady state (HHS). In contrast, the pituitary model is a fold-subHopf burster, because the active phase begins at a fold (LP) and terminates at a sub-critical Hopf bifurcation (H). Note that, strictly speaking, it is the branch of unstable limit cycles associated with the active phase, and not necessarily the active phase itself that terminates at H, as seen in Fig. 2(d). The branch of unstable limit cycles begins at a homoclinic orbit of the saddle steady state (HHS) that lies in between LP and H.

Fig. 3(a) shows the phase portrait in the (V,n)-plane of the fast subsystem of the Chay-Keizer model with $Ca = 0.55$. The high-voltage state (the stable limit cycle Γ) has a large basin of attraction with a neck that is near the low-voltage steady state x_l. Specifically, Fig. 3(a) suggests that arbitrarily brief pulses can cause upward resetting provided I_{app} is large enough.

Figs. 3(b and c) show projections of the three-dimensional phase portraits into the (V,n)-plane of the fast subsystem of the pituitary model with $Ca = 0.55$ and $Ca = 1.0$, corresponding to Regions I and II in Fig. 2(d), respectively. In addition to the steady states x_h, x_l, and x_s and the one-dimensional unstable manifolds $W^u(x_s)$ of the saddle steady state x_s, we project a one-dimensional slice, denoted $\overline{W}^s(x_s)$, of the two-dimensioal stable manifold of $W^s(x_s)$ of x_s. In order to obtain a truthful relative location with respect to $W^u(x_s)$, we slice the two-dimensional manifold with a plane through the three steady states and project this slice onto the (V,n)-plane. The stable manifold acts as a basin boundary in Fig. 3(b), but plays no role in separating

the two stable steady states in Fig. 3(c). The basin boundary for $Ca = 1.0$ is the stable manifold of the periodic orbit; note that only the projection of the periodic orbit is shown in Fig. 3(c). See Figs. 6 and 8 for corresponding images in the three-dimensional phase space.

Fig. 3(b) is similar to Fig. 3(a), with the stable limit cycle replaced by the high-voltage steady state. In Fig. 2(c), the projected basin of attraction of the high-voltage steady state shrinks to a small circle and there is no neck. Therefore, upward resetting is no longer possible if instantaneous pulses are used, but it is possible with sufficiently long pulses that allow m_{L} and, especially, n to increase. To the right of H, it becomes even more difficult to reset, because the high-voltage steady state becomes unstable (i.e., the basin shrinks to a point); we limit our discussion to regions I and II as the trajectories do not extend past H with the parameters we have chosen. These two-dimensional projections lead us to expect that, whereas it is easy to reset the Chay-Keizer model throughout the silent phase of the bursts, the pituitary model will have trouble, at least in region II. (Resetting downwards from active phase to silent phase is easy and the same for both models, so we do not address that.)

It is not obvious, however, if the two-dimensional projections are sufficient to predict the effect of upward resetting for the three-dimensional subsystem (1)–(3) of the pituitary model. For example, in Region II, the unstable periodic orbit Γ cannot be the boundary of the basin of attraction of the high-voltage steady state. In three dimensions the basin boundary is formed by the two-dimensional stable manifold $W^s(\Gamma)$, which could widen very quickly and create a much larger basin of attraction that could make upward resetting just as easy as for the Chay-Keizer model. On the other hand, $W^s(\Gamma)$ could also form an even smaller basin that could virtually preclude resetting. In order to assess the difficulty of upward resetting in the fast subsystem of the pituitary model, it is necessary to calculate the two-dimensional surface that separates the basins of attraction of the low- and high-voltage steady states. Recently, techniques have been developed that allow to compute two-dimensional separating manifolds (see Section 2 for references). We describe the results of these techniques and of resetting simulations in the next section.

3.2 Resetting in the frozen system

Fig. 4(a) shows how the bifurcation diagram of Fig. 2(d) is altered when a constant-current pulse $I_{\mathrm{app}} = 6.69$ is applied and maintained indefinitely. Two things happen: the fold LP is pulled to the right, allowing the phase point to escape, and a new high-voltage steady state is created. If the applied current is not too large, there is a good chance that the new steady state will lie in the basin of attraction of the old high-voltage state, leading to a successful reset. If the current is too large, the high-voltage state will move out of the basin of attraction of the unperturbed high-voltage state. As an example, consider upward resetting from $Ca = 1.0$. Fig. 4(b) shows how the steady states and periodic orbit for $Ca = 1.0$ depend on I_{app}. For small enough I_{app} the low-voltage steady state persists, but it disappears in a fold (LP) at $I_{\mathrm{app}} \approx 6.49$ pA and for larger I_{app} escape from the silent phase is possible at $Ca = 1.0$, as shown in Fig. 4(a); the vertical line in Fig. 4(b) shows that for $I_{\mathrm{app}} = 6.69$ only a high-voltage steady

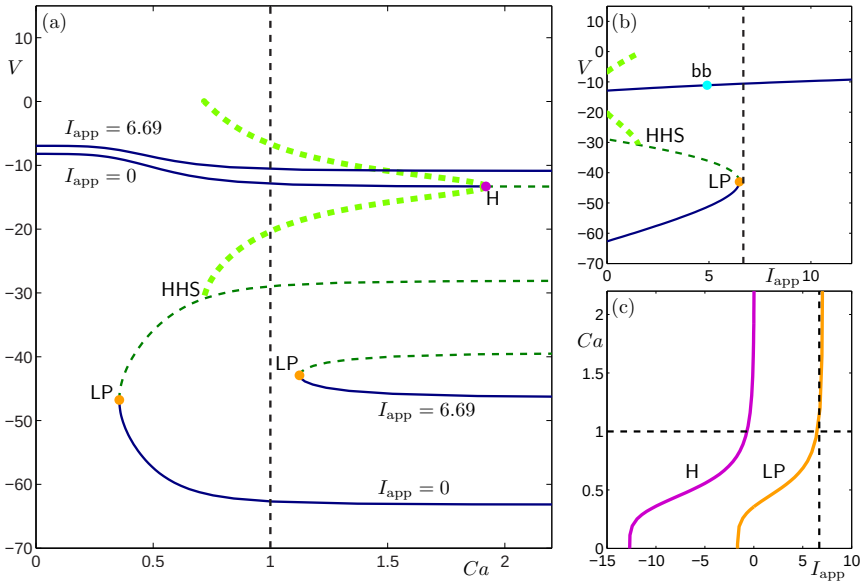

Fig. 4 Influence of applied current I_{app} on the fast subsystem of the pituitary model. Panel (a) shows how the bifurcation diagram for $I_{app} = 0$ changes when I_{app} is increased to 6.69 pA. The Hopf bifurcation H for $I_{app} = 0$ has disappeared altogether. Panel (b) shows how the equilibria and periodic orbits for $Ca = 1.0$ μM vary with I_{app}. The dot labeled bb indicates the value of I_{app} at which the perturbed depolarized state leaves the basin of attraction of the unperturbed state. Panel (c) shows how the fold and Hopf bifurcation curves vary in (I_{app}, Ca)-space.

state exists. Note that the periodic orbit disappears in a homoclinic bifurcation (HHS) well before the fold. The point labeled bb on the branch of high-voltage steady states in Fig. 4(b) lies on the boundary of the basin of attraction of the unperturbed high-voltage steady state and marks the minimum value of I_{app} that is large enough for the high-voltage state to lie outside this basin of attraction. As shown in Fig. 4(b), for any value of I_{app} large enough to cause escape from the low-voltage state, the asymptotic limit of the trajectory lies outside the basin for resetting upwards. It is still possible to achieve a reset if the orbit transiently passes through the basin and the current is turned off in time, but this is more delicate. For smaller Ca, the minimum value of I_{app} decreases because the inhibitory effect of Ca on V via the BK channels is smaller. This is summarized in Fig. 4(c). Putting the three views together suggests that resetting should be easiest in region I, where the basin of attraction is larger and the minimum value for I_{app} is lower.

Let us now study what happens to the (unperturbed) low-voltage steady state in the fast subsystem (1)–(3), for a fixed value of Ca, if we apply a constant current pulse I_{app} only for a finite duration w. Fig. 5 shows the applied current strength-duration relationship determined by forward integrations on a grid of (I_{app}, w)-values for $Ca = 0.55$ μM; the figure is representative for Ca values in region I as indicated in Fig. 2(d). The two-parameter bifurcation diagram in Fig. 4(c) predicts that for this value of Ca, resets are not possible for $I_{app} < 3.35$ pA because the pulse is too weak

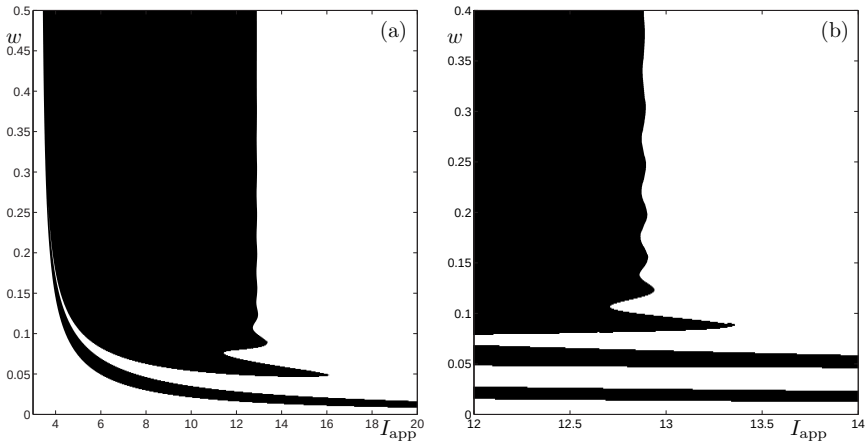

Fig. 5 Strength-duration diagram constructed by forward integrations for 10 s of the fast subsystem with $Ca = 0.55$ μM, starting at the low-voltage steady state. Points in the black region correspond to values of pulse strength $I_{\rm app}$ and pulse duration w that give rise to successful resets (i.e. the associated trajectories terminate at the high-voltage steady state). The grid resolution was 0.001 pA $\times$ 0.001 s. A minimum value of $I_{\rm app}$ is needed for the phase point to be captured in the basin of attraction of the high-voltage steady state (a). For larger values of $I_{\rm app}$, there is a minimum duration w for success. For $I_{\rm app} >\approx 12.87$ pA there is also a maximum value of w generating successful capture (b).

to drive the fold (LP) beyond $Ca = 0.55$ μM. The results of forward integration are consistent with this, showing no resets for $I_{\rm app} < 3.376$ pA with stimulus durations up to 1 s (the results in Fig 5(a) are displayed for $w \leq 0.5$ s). For $3.35 \leq I_{\rm app} <\approx 12.87$ pA the perturbed system has a unique steady state that lies in the basin of attraction of the high-voltage steady state of the unperturbed system. In this range, resetting is guaranteed provided the duration is long enough. With forward integrations, we found successful resets for all sufficiently long pulses for $3.376 \leq I_{\rm app} < 12.886$ pA, which agrees with the prediction given the accuracy with which we can calculate the manifold that forms the basin boundary. Note further that there is a horizontal band of failures; in this region the trajectory winds transiently out of the basin. If the pulse is maintained a little longer, however, the reset is successful. For $I_{\rm app} > 12.87$ pA, the induced high-voltage steady state lies outside of the basin, and resetting is not possible except for a narrow strip corresponding to the time when the trajectory transiently passes through the neck of the basin. Such delicate resets are possible for arbitrarily large $I_{\rm app}$, but the window of duration shrinks to 0. Thus, in practice resetting is not possible for large $I_{\rm app}$ and would appear as an overshoot, i.e., V would go above the unperturbed plateau but would not stay up significantly longer than the pulse.

The most interesting region is the wavy boundary that straddles the line $I_{\rm app}$ = 12.87 pA; an enlargement is shown in Fig. 5(b). For any $I_{\rm app}$ in this region, failures alternate with successes as the trajectory winds in and out of the basin of attraction on the way to the induced high-voltage steady state. There can be failures when the induced high-voltage state lies inside the basin, because the trajectory leaves the basin transiently on the way to this induced high-voltage steady state, and there can be

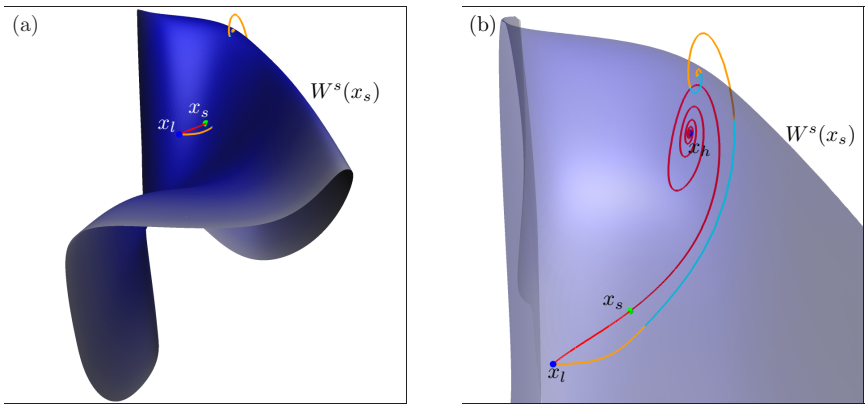

Fig. 6 Three-dimensional phase portrait of the fast subsystem with $Ca = 0.55$ μM. The V axis is horizontal. The *blue* surface in panel (a), which is rendered transparent in panel (b), is the stable manifold $W^s(x_s)$ of the saddle steady state x_s (see also Fig. 3(b)) and defines the basin boundary of the high-voltage steady state x_h. *Red* curves are the unstable manifolds of x_s (*green* dot). Shown in *orange* is the trajectory for $I_{\text{app}} = 12.87$ pA, with segments that lie inside the basin of attraction shown in *cyan*. A large enough applied current I_{app} will move the system out of the low-voltage steady state x_l, so that only very specific durations capture the trajectory inside the basin of attraction of x_h.

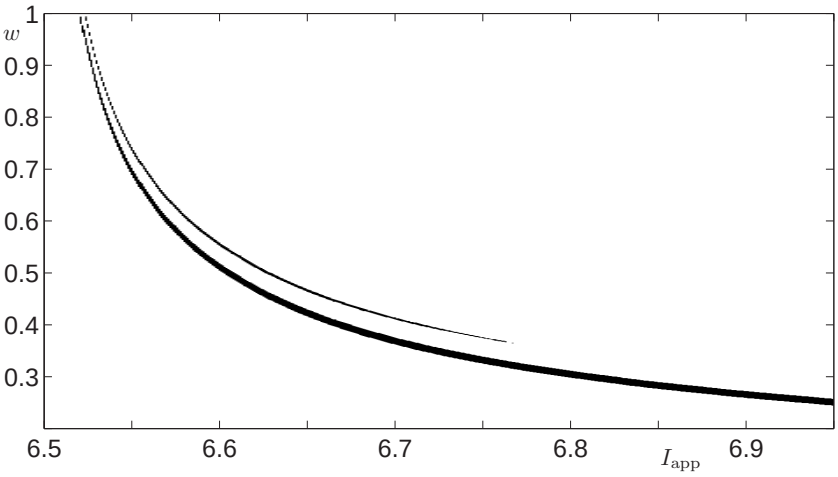

Fig. 7 Strength-duration diagram of the fast subsystem as in Fig. 5 but with $Ca = 1.0$ μM (region II in Fig. 2(d)). A minimum value for I_{app} is needed for the trajectory to be captured in the basin of attraction of the high-voltage steady state. There is also a maximum value of I_{app} for which this can be achieved (not shown).

successes when the steady state lies outside the basin but the trajectory enters the basin transiently. Fig. 6 shows an example taken from the wavy region with $I_{\text{app}} = 12.87$ pA, the value where the induced high-voltage steady state lies approximately on the boundary of the basin. On the way to the induced high-voltage steady state, the trajectory winds in (*cyan*) and out (*orange*) of the basin.

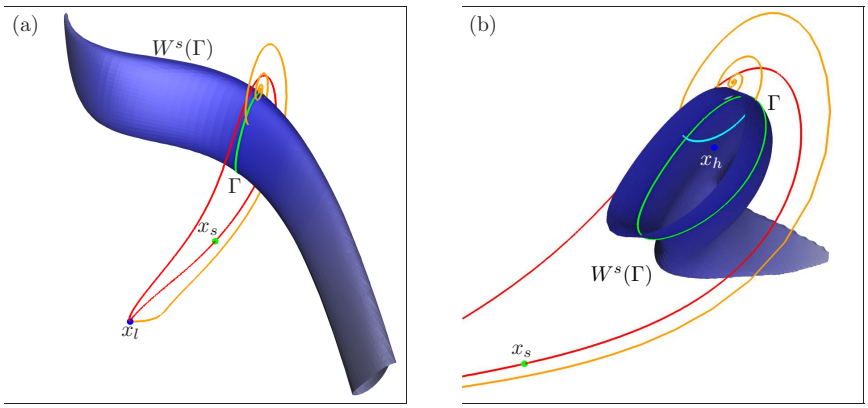

Fig. 8 Three-dimensional phase portrait of the fast subsystem with $Ca = 1.0\ \mu$M. Colors are as in Fig. 6 but now the basin boundary (*blue surface*) is the stable manifold $W^s(\Gamma)$ of the unstable periodic orbit Γ (*dark green* curve). The horizontal axis is V in panel (a), while the view is rotated in panel (b) and part of the basin boundary chopped off so one can see inside. Any applied current I_{app} large enough to move the system out of the low-voltage steady state x_l will converge to a point outside the basin of attraction of the high-voltage steady state x_h. Shown in *orange* is the trajectory for $I_{\text{app}} = 6.69$ with segments that lie inside the basin of attraction shown in *cyan*. *Red* indicates the unstable manifolds $W^u(x_s)$ of x_s (*green* dot).

We next examine the strength-duration relationship for $Ca = 1.0\ \mu$M (Fig. 7), which is in region II. In this region, any stimulus strong enough to move the trajectory out of the silent phase is strong enough to move the induced high-voltage steady state out of the basin of the unperturbed high-voltage steady state, which is in any case much smaller than in region I. That is, any value of I_{app} to the right of the fold LP in Fig. 4(b) is also to the right of the dot labeled bb at which the induced high-voltage steady state first leaves the basin. Thus, the only possibility of resetting is for the trajectory to visit the basin transiently, which leads to the narrow bands in Fig. 7.

Fig. 8 shows a resetting trajectory with $I_{\text{app}} = 6.69$ pA superimposed on the phase portrait with the two-dimensional manifold that forms the basin boundary, with frozen $Ca = 1.0\ \mu$M. In this example the induced high-voltage steady state lies outside the basin of attraction of the unperturbed high-voltage steady state. The *cyan* portions of the trajectory that are visible in Fig. 8b indicate successful resets when the basin is transiently visited and correspond to values of duration in the two black bands in Fig. 7. Fig. 8 also gives an impression of the effect of the additional gating variable m_L in the model. The resetting trajectory clearly moves away from the plane through the steady states x_l, x_s, and x_h, while the saddle periodic orbit Γ lies almost entirely in this plane. If the basin boundary $W^s(\Gamma)$ had had more of a trumpet shape, successful resetting would have been achieved by arbitrarily brief pulses, just as for the Chay-Keizer model.

3.3 Resetting in the full system (*Ca* dynamic)

We now examine resetting in the full four-dimensional system (1)–(4) in which Ca is a slow variable rather than a frozen parameter. This is the situation that corresponds to

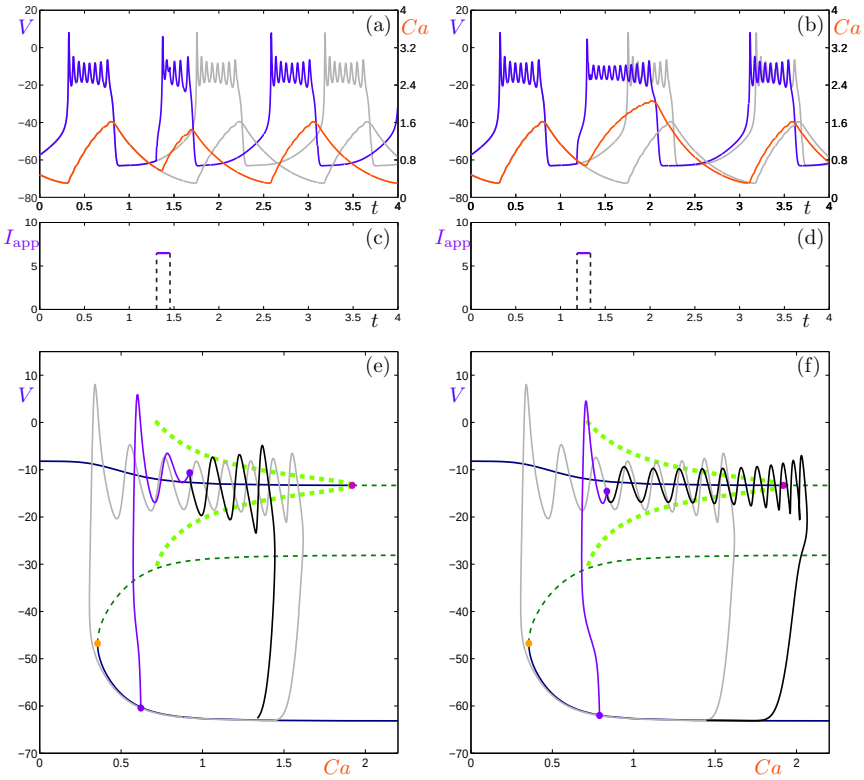

Fig. 9 Phase-resetting profiles with applied current $I_{app} = 6.48$ pA and duration $w = 0.15$ s initiated at a late (left column) and early (right column) state in the silent phase. Panels (a) and (b) show V (*purple*, left axis) and Ca (*orange*, right axis) versus t with I_{app} versus t underneath in panels (c) and (d). Panels (e) and (f) show these as orbits in the (Ca,V)-plane overlaid on the corresponding bifurcation diagram of the fast subsystem. The start and end of the pulse is indicated by a *thick dot*, and the unperturbed oscillation is shown in *light grey*.

the experimental setting and hence is in principle testable. The analysis of the frozen system suggests that it should be relatively easy to reset upwards at late points in the silent phase for which the frozen system lies in region I (Figs. 5 and 6), and nearly impossible to reset at early points in the silent phase, for which the frozen system lies in region II (Fig. 7 and 8). However, the dynamics of Ca complicate the picture.

Fig. 9 shows examples of successful resetting of the full system in the time domain (a and b) and in the (Ca,V) phase plane (e and f). Success is defined as an induced plateau that outlasts the applied current (Fig. 9(c and d)). The left panels (a, c, e) show an example late in the silent phase, when the frozen system lies in region I. A subtlety that does not arise in the frozen system is that if the duration of the applied current is too long, Ca can increase, pulling the trajectory into region II. Thus, even though the induced high-voltage steady state lies in the basin for this value of I_{app}, the current cannot be maintained too long, because the rise in Ca will deform the manifolds and shrink the basin of attraction.

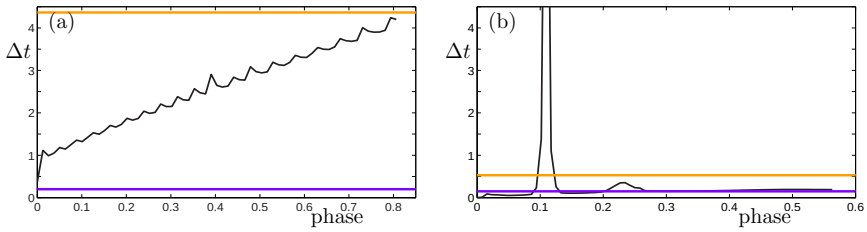

Fig. 10 Phase-resetting diagrams for the Chay-Keizer model with $I_{app} = 2$ pA, $w = 0.2$ s (a) and the pituitary model (b) with $I_{app} = 6.48$ pA, $w = 0.15$ s. Plotted is the return time to low-voltage values ($V = -55$ mV for Chay-Keizer and $V = -30$ mV for the pituitary model) after resetting at the given phase, that is, the time relative to the duration of the silent phase. The upper (*orange*) horizontal line indicates the duration of the unperturbed active phase and the lower (*purple*) horizontal line indicates the duration of the current pulse. The large peak in panel (b) is cut off to keep the smaller peak visible; the maximal Δt is 13.3 s.

The right panels (b, d, f) of Fig. 9 show an example of resetting early in the silent phase, when the frozen system lies in region II. In this case, *Ca* initially decreases because the phase point lies below the *Ca* null surface. This increases the size of the basin of attraction, and allows the reset to succeed, even though the frozen picture suggests that it would fail. Note that in this example, the induced plateau is longer than the unperturbed plateau.

Fig. 10(a) shows how the duration of the induced excursion varies with the point in the silent phase at which the pulse is applied for the Chay-Keizer model. Broadly, the later the pulse is applied, the longer is the induced active phase. (The curve is not monotonic because there is a bump every time a spike is added. The spike-adding canard bifurcation is described by Terman (1991).)

The increase of excursion length with phase of reset is not surprising as at later times the trajectory is closer to where it would jump up anyway. In contrast, Fig. 10(b) shows that resetting does not necessarily become easier later in the silent phase for the pituitary model. Resetting is only successful during narrow windows of the silent phase because of the influence of the *Ca* dynamics on the manifolds of the frozen system. Remarkably, the successful resets can be much longer than the duration of the unperturbed active phase, a phenomenon that is never seen in the Chay-Keizer type models. Also, the left (stronger) peak corresponds to the situation in Fig. 9(b and d), in which the reset trajectory begins in region II — the frozen analysis predicted that resetting would be difficult for this region — whereas the right (weaker) peak corresponds to Fig. 9(a and c), in which the trajectory begins in region I.

4 Discussion

We have considered two classes of candidate models for a particular flavor of pseudo-plateau bursting observed so far in several pituitary cell types (Kuryshev et al 1996; Stojilkovic et al 2005) and at times in isolated pancreatic β-cells (Kinard et al 1999). These bursts are relatively brief (a few seconds) and have small-amplitude spikes that are suggestive of fluctuations rather than full-blown action potentials. The classical

model for square-wave bursters, developed first by Chay and Keizer (1983) for pancreatic β-cells (when studied in coupled islets of Langerhans) and later applied to other cell types, such as respiratory pacemaker neurons (Butera et al 1999), and to networks of neurons (Tabak et al 2000), is classified as fold-homoclinic based on how the active phase begins and terminates (Izhikevich 2000). As an alternative, we have presented here a model classified as fold-subHopf (Izhikevich 2000) because the branch of limit cycles associated with the active phase ends at a sub-critical Hopf bifurcation (Fig 2d); the termination of the active phase itself is more complex, as discussed below.

A diagram with fold-subHopf structure was exhibited using a particular parameter set for the original corticotroph model from which the present model was derived (LeBeau et al 1998, Fig. 13). A recent model for pituitary lactotrophs has also been shown to have the same structure (Tabak et al 2007, Fig. 3). Finally, the gonadotroph model of van Goor et al (2001) has the same structure when shifted into a pseudo-plateau bursting mode by "transfection" of a large-conductance Ca^{2+}-activated K^+ channel (unpublished observations). The investigation of the properties of this class of models is in its infancy, but it is already clear that they are rather different from and more complex than those of the older fold-homoclinic class in many respects. (See for example some of the counter-intuitive effects of changing calcium pump rates in Tabak et al, 2007.)

4.1 Summary of results

In this study we have focused on the response to resetting pulses, which has not been addressed previously. We have only discussed in detail upward resetting from the silent phase to the active phase, as the properties of downward resetting do not differ significantly between the two classes of models. The differences in the properties of upward resetting, on the other hand, do provide a clear-cut experimental signal for choosing whether a fold-homoclinic or a fold-subHopf model is more appropriate for a given system. (There could be other types of models that work even better, so the determination is only relative; see caveats below.)

We first considered resetting with the slow variable, cytosolic calcium (*Ca*), frozen and identified two distinct regions, labeled I and II in Fig. 2(d). Consideration of two-dimensional projections of the three-dimensional fast subsystem suggested that in Region I, between the lower knee (LP) and the homoclinic orbit (HHS), resetting would be relatively easy as the projected basin of attraction is large and contains both the low- and high-voltage steady states (Fig. 3(b)). In contrast, in Region II, between the homoclinic orbit (HHS) and the Hopf bifurcation (H), resetting was expected to be more difficult as the projected basin is very small, shrinking to a point as H is appproached (Fig. 3(c)).

Confirmation of these predictions required calculation of the three-dimensional phase portraits. In region I, forward integrations showed that resetting is possible for sufficiently prolonged depolarizing stimuli, as long as the current strength is not so great that it pushes the high-voltage steady state of the perturbed system out of the basin of attraction of the unperturbed high-voltage steady state (Fig. 5). In re-

gion II, we found that any stimulus strong enough to escape the low-voltage steady state pushes the induced high-voltage steady state out of the basin. Hence, resets are possible only in very narrow bands of duration (Fig. 7). The two-dimensional separating manifolds that bound the basins of attraction of the high-voltage steady state gave further information about the conditions for success of upward resetting with a constant-current pulse of a given strength and duration when they were overlaid with the trajectory generated by a pulse of this strength with infinite duration. Specifically, they showed that the wavy border of the resetting region in Fig. 5 and the narrow bands in Fig. 7 were due to the reset trajectory repeatedly intersecting the manifolds (Figs. 6, 8).

In the full four-dimensional system, with *Ca* dynamic, the situation is more complex because the dynamics of *Ca* deforms the basin of attraction of the high-voltage steady state and can drive a reset trajectory that begins in region I into region II and *vice versa*. The end result is that resetting is difficult whether initiated in either region, with one narrow window of propitious phases corresponding roughly to each region (Fig. 10(b)). Surprisingly, resets initiated in region II, expected to be more difficult based on the frozen analysis, led to much longer excursions that could exceed the native active-phase duration by an order of magnitude. This is dramatically different from the situation in the fold-homoclinic burster, where resetting is possible throughout the silent phase and the excursion durations are generally bounded by the native active-phase duration (Fig. 10(a)).

4.2 Robustness of results

We believe that the three-dimensional fast subsystem is representative for the dynamics of possibly more detailed higher-dimensional models of a pituitary cell. Any additional variable in the model would have faster kinetics than m_L, which already has fast kinetics relative to n. This relatively faster kinetics of m_L causes the flow to compress rapidly towards the high-voltage steady state, rendering the flow nearly two-dimensional. *A priori* one might expect differences between a three-dimensional fast subsystem and a two-dimensional reduced version, obtained by setting the L-type Ca^{2+} channel activation variable m_{L} to steady state, because the basin of attraction of the high-voltage steady state, bounded by the stable manifold of the saddle periodic orbit surrounding it, could bend significantly as one moves transverse to the periodic orbit. However, we have checked that such a reduced version of the pituitary model with a two-dimensional fast subsystem qualitatively shows the same pattern of dynamic resetting as shown in Fig. 10(b). Whether there are genuine differences between the two- and three-dimensional cases beyond the aspects we have examined is an open question.

The marked difference in resetting patterns between fold-homoclinic and fold-subHopf does not depend on the choice of the resetting parameters I_{app} and w; we find the same pattern of strong and weak resets if either pulse strength or duration is varied over a wide range and the other parameter is kept fixed (not shown). The results can, however, depend on model parameters if these influence the locations of the homoclinic and Hopf bifurcations relative to the fold. In the case considered here,

the time spent in regions I and II is comparable. If region I is enlarged by moving the homoclinic bifurcation to the right, resetting becomes easier and begins to exhibit a pattern similar to the fold-homoclinic burster. We have observed this for a closely related model (Tsaneva-Atanasova et al 2007) in which region II is very small.

4.3 Mathematical directions

An issue for further analysis is precisely how the active phase is terminated. Although the model is classified as fold-subHopf by the criteria of Izhikevich (2000), the active phase ends well before the Hopf bifurcation is reached. In the model of Tsaneva-Atanasova et al (2007), where the Hopf bifurcation is right-shifted, the active phase ends even before the homoclinic orbit. On the other hand, in the two-dimensional reduced version of the model, the trajectory approaches the high-voltage steady-state branch more rapidly. Because of this compression, the trajectory can tunnel through the Hopf bifurcation and stay up for a significant time and distance even though there is no stable steady state to support it (see also Izhikevich 2000, Fig. 103). Similar behavior is seen in subHopf-fold cycle bursters (Izhikevich 2000, Fig. 80), also known as "elliptic" bursters. This tunneling phenomenon (Baer and Rinzel 1988) is responsible for the exceptionally long resets recorded in Fig. 10(b), a mild example of which is shown in Fig. 9(b and d). The ratio of the speed of the slow variable to the strength of attraction of the high-voltage steady state would seem to be an important parameter in determining where the active phase ends. The exit from the active phase also depends on how the trajectory intersects the basin of attraction, which may be complex due to the wrapping of the basin around the high-voltage steady state. Furthermore, the manifolds deform as Ca varies, making it difficult to predict the exit from the frozen system, just as it was difficult to predict the dynamic resets from the frozen system. Analyzing the full four-dimensional system may be necessary (cf. Terman 1991).

If the Hopf bifurcation is moved to the left, towards the fold, the active phases become shorter, and the spikes become taller. Eventually, bistability is lost as the homoclinic orbit coalesces with the fold to form a saddle-node loop. This is proposed in Tsaneva-Atanasova et al (2007) as an explanation for both the natural variability of burst periods in somatotrophs and the conversion of pseudo-plateau bursting to beating by block of BK Ca^{2+}-activated K^+ channels (van Goor et al 2001). In the model presented here, which lacks BK channels, the same transition can be achieved by increasing the time constant τ_n of the voltage-dependent K^+ channel or increasing the conductance g_{CaL} of the L-type Ca^{2+} channel. The same parameter manipulations convert the Chay-Keizer model from a fold-homoclinic burster to a beater, but it does not seem possible to compose the two transformations to convert fold-subHopf to fold-homoclinic; at least one additional parameter change is required. It would be of interest to determine if there is a simple way to carry out this conversion, as this might indicate how close the two classes of bursters are in parameter space. That is, in spite of the similar appearance, they may actually be far apart in the sense of plausible biophysical modifications. The unfolding approach of Golubitsky et al (2001) may be helpful here.

4.4 Caveats and guidance for experimental testing

For the benefit of those who may be interested in testing the predictions of the model, we summarize the key results and give some supplementary advice.

The basic conclusion from the study is that one can determine which of the two classes of bursting models considered here is more appropriate for a given cell type or preparation. In one type the spikes are generated by slowly modulated stable oscillations whereas in the other they are generated by transients. In the latter case, it is much more difficult to reset the oscillations from the silent phase to the active phase because the basin of attraction of the depolarized state is much smaller. However, in the rare cases when success is achieved, the induced active phases may significantly exceed the duration of the native active phase (Fig. 10(b)). A limitation of the test proposed here is that it is one-sided: it is possible for a model with transient spikes to show a resetting pattern similar to that of the classical square-wave burster so the test is only decisive if a pattern of Fig. 10(b) is observed. We expect the pattern of Fig. 10(a) in cases where the high-voltage steady state is stable throughout the active phase (i.e. the fold-fold burster described above), and we have seen it in a model that is close to fold-fold (Tsaneva-Atanasova et al 2007). Resetting from the active phase to the silent phase should be similarly easy in all the above types of models and can be used as a positive control to test that the protocols are working.

Another prediction of the study, which applies to both classes of models is that pulses that are too strong or too long will result in failures to reset because the trajectory overshoots the high-voltage steady state. This is not obvious from purely biophysical considerations, and in fact, similar failures do not occur when resetting from active to silent phase. Because it tends to be harder to reset in the early part of the silent phase, failures may be detected early when late resets are still successful; this may be an indication to reduce the stimulus strength or duration slightly. Note that overshoots are predicted for both the Chay-Keizer type model and the pituitary model, so this phenomenon is itself of interest independent of the class of burster.

Since the spikes in the type of model described here are generated by transient oscillations decaying to a steady state, one would not expect the model to apply to cells with very long bursts; if the burst duration is long compared to the kinetics of cytosolic calcium, the membrane potential would have enough time to settle down to a plateau without spikes. Thus, likely candidates to be fit by the pituitary model are cases in which the bursts are relatively short and the spike amplitude is small. Conversely, one might expect cells with larger spike amplitude to be much slower than the pituitary cells that motivated this study. A cautionary exception to this inference is the pre-Bötzinger pacemaker neuron, but note that in those cells, the function of the somatic spikes is to drive Na^+-mediated action potentials down the axon to the nerve terminal, not to drive Ca^{2+} entry directly into the soma.

The emphasis here has been on the dynamical structures of the models rather than the more usual approaches of comparing appearance of the output or biophysical mechanisms (e.g. Stojilkovic et al 2005). It is entirely possible for cells to achieve the same structure with different ion channels or different structures with the same ion channels. Thus, the tests choose between classes of models rather than models *per se*.

Acknowledgements This work was supported in part by the intramural research program of the National Institute of Diabetes and Digestive and Kidney Diseases, National Institutes of Health. HMO acknowledges the hospitality and support of the Laboratory of Biological Modeling. The research of HMO was supported by an Advanced Research Fellowship grant from the Engineering and Physical Sciences Research Council (EPSRC).

Appendix: Model Equations

In addition to the four differential equations (1)–(4) given in section 2, the ionic currents and auxiliary expressions given below are needed to complete the specification of the model.

The ionic currents are:

– L-type Ca^{2+} current

$$I_{\mathrm{CaL}} = g_{\mathrm{CaL}} m_{\mathrm{L}}^2 (V - V_{\mathrm{Ca}}); \tag{5}$$

– T-type Ca^{2+} current

$$I_{\mathrm{CaT}} = g_{\mathrm{CaT}} m_{\mathrm{T},\infty}^2(V) h_{\mathrm{T},\infty}(V)(V - V_{\mathrm{Ca}}); \tag{6}$$

– Voltage-dependent K^+ current

$$I_{\mathrm{K}} = g_{\mathrm{K}} n (V - V_{\mathrm{K}}); \tag{7}$$

– Leak current

$$I_{\mathrm{Leak}} = g_{\mathrm{Leak}} (V - V_{\mathrm{Leak}}); \tag{8}$$

The leak stands in for a variety of subthreshold currents that play important modulatory roles in models for specific pituitary cell types. Such currents include the A-type K^+ current, which has been suggested to mediate the effects of dopamine in lactotrophs (Tabak et al 2007), and the inward-rectifier K^+ current and the cyclic-nucleotide gated non-selective cation current, which have been suggested to mediate the effects of somatostatin and growth hormone releasing hormone in somatotrophs (Tsaneva-Atanasova et al 2007).

– Ca^{2+}-activated K^+ current

$$I_{\mathrm{KCa}} = g_{\mathrm{KCa}} \frac{Ca^4}{Ca^4 + K_{\mathrm{KCa}}^4} (V - V_{\mathrm{K}}); \tag{9}$$

In particular cell models, this current has been suggested to be the small-conductance (SK) channel (Tabak et al 2007; van Goor et al 2001) or the current through a subset of the big-conductance (BK) channels (Tsaneva-Atanasova et al 2007).

The steady-state activation functions take the form

$$X_\infty(V) = \frac{1}{1 + \exp(-(V - V_X)/k_X)}, \tag{10}$$

with $X = m_{\mathrm{L}}, m_{\mathrm{T}}, h_{\mathrm{T}},$ and n. The time functions are constants except for

$$\tau_{\mathrm{m,L}}(V) = \frac{\bar{\tau}_{\mathrm{m,L}}}{\exp((V - V_\tau)/k_\tau) + 2\exp(-2(V - V_\tau)/k_\tau)}. \tag{11}$$

The calcium balance equation Eq. (4) has a term for exchange between the cytosol and the internal (endoplasmic reticulum) store,

$$J_{\text{exchange}} = \frac{Ca_{\text{eq}} - Ca}{\tau_{\text{Ca}}}, \tag{12}$$

a term for influx through calcium channels,

$$J_{\text{influx}} = -\alpha(I_{\text{CaL}} + I_{\text{CaT}}), \tag{13}$$

and a term for pumping calcium out of the cell,

$$J_{\text{efflux}} = v_{\text{P}} \frac{Ca^2}{Ca^2 + K_{\text{P}}^2}. \tag{14}$$

The factors α in Eq. (13) and β in Eq. (4) combine to convert units of flux to units of current (see Table 1).

References

Baer SM, Rinzel J (1988) Threshold for repetitive activity for a slow stimulus ramp: a memory effect and its dependence on fluctuations. Biophys J 54(3):551–555

Bertram R, Butte M, Kiemel T, Sherman A (1995) Topological and phenomenological classification of bursting oscillations. Bull Math Biol 57:413–439

Butera R Jr, Rinzel J, Smith JC (1999) Models of respiratory rhythm generation in the pre-Bötzinger complex. I. bursting pacemaker neurons. J Neurophysiol 82(1):382–397

Chay TR, Keizer J (1983) Minimal model for membrane oscillations in the pancreatic β-cell. Biophys J 42:181–190

Doedel E (1981) AUTO: A program for the automatic bifurcation analysis of autonomous systems. Cong Num 30:265–284

England JP, Krauskopf B, Osinga HM (2007) Computing two-dimensional global invariant manifolds in slow-fast systems. International Journal of Bifurcation and Chaos X(Y):in press

Ermentrout B (2002) Simulating, Analyzing, and Animating Dynamical Systems. SIAM, Philadelphia, PA

Golubitsky M, Josic K, Kaper TJ (2001) An unfolding theory approach to bursting in fast-slow systems. In: Broer H, Krauskopf B, Vegter G (eds) Analysis of Dynamical Systems: Festschrift dedicated to Floris Takens on the occasion of his 60th birthday, Institute of Physics Publ, Bristol, pp 277–308

van Goor F, Li YX, Stojilkovic S (2001) Paradoxical role of large-conductance calcium-activated K^+ (BK) channels in controlling action potential-driven Ca^{2+} entry in anterior pituitary cells. J Neurosci 21:5902–5915

Izhikevich EM (2000) Neural excitability, spiking, and bursting. International Journal of Bifurcation and Chaos 10:1171–1266

Kinard TA, de Vries G, Sherman A, Satin LS (1999) Modulation of the bursting properties of single mouse pancreatic β-cells by artificial conductances. Biophys J 76:1423–1435

Krauskopf B, Osinga HM (2003) Computing geodesic level sets on global (un)stable manifoldsof vector fields. SIAM J Appl Dyn Sys 2(4):546–569

Krauskopf B, Osinga HM, Doedel EJ, Henderson ME, Guckenheimer JM, Vladimirsky A, Dellnitz M, Junge O (2005) A survey of methods for computing (un)stable manifolds of vector fields. SIAM J Appl Dyn Sys 15(3):763–791

Kuryshev YA, Childs GV, Ritchie AK (1996) Corticotropin-releasing hormone stimulates ca entry through l- and p-type ca channels in rat corticotropes. Endocrinology 137(6):2269–2277

LeBeau AP, Robson AB, McKinnon AE, Sneyd J (1998) Analysis of a reduced model of corticotroph action potentials. J theor Biol 192:319–339

Lisman J (1997) Bursts as a unit of neural information: making unreliable synapses reliable. Trends Neurosci 20(1):38–43

Parameter	Description	Value or Definition
d_{cell}	cell diameter	10 μm
A_{cell}	cell surface area	314.16 μm^2
V_{cell}	cell volume	523.5 μm^3
f	fraction of free calcium	0.01
α	$\frac{1}{z_{\text{Ca}}FA_{\text{cell}}}$; F is Faraday's constant	16.49 μM μm nA^{-1} s^{-1}
β	$\frac{A_{\text{cell}}}{V_{\text{cell}}}$	0.6 μm^{-1}
C_m	capacitance	0.00314 nF
V_{Ca}	calcium reversal potential	60 mV
V_{K}	potassium reversal potential	-80 mV
g_{CaL}	L-channel conductance	1.366 nS
g_{CaT}	T-channel conductance	0.001 nS
g_{K}	V-dependent K channel conductance	4.1 nS
g_{KCa}	KCa channel conductance	0.25 nS
K_{KCa}	Ca for half-maximal KCa activation	0.5 μM
g_{Leak}	Leak conductance	0.3 nS
V_{Leak}	Leak reversal potential	-50 mV
V_m	V for half-max L-channel activation	-25 mV
k_m	L-channel slope factor	12 mV
$V_{m_{\text{T}}}$	V for half-max T-channel activation	-45 mV
$k_{m_{\text{T}}}$	T-channel activation slope factor	8 mV
$V_{h_{\text{T}}}$	V for half-max T-channel inactivation	-52 mV
$k_{h_{\text{T}}}$	T-channel inactivation slope factor	-5 mV
V_n	V for half-max K channel activation	5 mV
k_n	K channel activation slope factor	8 mV
V_τ	L-channel time function reference V	-60 mV
k_τ	L-channel time function slope factor	22 mV
$\bar{\tau}_{\text{m,L}}$	L-channel time funtion scale factor	0.027 s
τ_n	K-channel time constant	0.02 s
ν_{P}	Maximal pump rate	40.0 μM μm s^{-1}
K_{P}	Ca for half-maximal pump activation	0.08 μM
τ_{Ca}	ER exchange time constant	0.5 s
Ca_{eq}	Background Ca	0.1 μM

Table 1 Parameter values for the pituitary model (1)–(4).

Phillips M, Levy S, Munzner T (1993) Geomview: An interactive geometry viewer. Notices Amer Math Soc 40:985, URL `http://www.geomview.org`

Rinzel J (1987) A formal classification of bursting mechanisms in excitable systems. In: Teramoto E, Yamaguti M (eds) Mathematical Topics in Population Biology, Morphogenesis, and Neurosciences, Springer-Verlag, New York, pp 267–281, lecture Notes in Biomathematics 71

Sherman A, Rinzel J, Keizer J (1988) Emergence of organized bursting in clusters of pancreatic β-cells by channel sharing. Biophys J 54:411–425

Stojilkovic SS, Zemkova H, van Goor F (2005) Biophysical basis of pituitary cell type-specific Ca^{2+} signaling-secretion coupling. Trends Endocrinol Metab 16(4):152–159

Tabak J, Senn W, O'Donovan MJ, Rinzel J (2000) Modeling of spontaneous activity in developing spinal cord using activity-dependent depression in an excitatory network. J Neurosci 20(8):3041–3056

Tabak J, Toporikova N, Freeman ME, Bertram R (2007) Low dose of dopamine may stimulate prolactin secretion by increasing fast potassium currents. J Comput Neurosci Epub ahead of print:DOI 10.1007/s10,827–006–0008–4

Terman D (1991) Chaotic spikes arising from a model of bursting in excitable membranes. SIAM J Appl Math 51:1418–1450

Tsaneva-Atanasova K, Sherman A, van Goor F, Stojilkovic SS (2007) Mechanism of spontaneous and receptor-controlled electrical activity in pituitary somatotrophs, in review